

15

**Lucija Hanžič, Jurij Karlovšek, Tomaž Hozjan, Sabina Huč, Zhongyu Xu,
Igor Planinc and Johnny C.M. Ho**

Experimental and numerical investigation of restrained shrinkage of concrete



EXPERIMENTAL AND NUMERICAL INVESTIGATION OF RESTRAINED SHRINKAGE OF CONCRETE

Lucija Hanžič^{1,2*}, Jurij Karlovšek², Tomaž Hozjan³, Sabina Huč^{3,1}, Zhongyu Xu², Igor Planinc³ and Johnny C.M. Ho⁵

¹ Slovenian National Building and Civil Engineering Institute (ZAG)
Dimičeva ulica 12, 1000 Ljubljana, Slovenia
e-mail: info@zag.si, * lucija.hanzic@zag.si

² The University of Queensland, School of Civil Engineering
Bldg. 49, Staff Rd, St Lucia QLD 4072, Australia
e-mail: enquiries@civil.uq.edu.au

³ University of Ljubljana, Faculty of Civil and Geodetic Engineering
Jamova cesta 2, 1000 Ljubljana, Slovenia
e-mail: tajnistvo@fgg.uni-lj.si

⁴ University of Ljubljana, Faculty of Chemistry and Chemical Technology
Večna pot 13, 1000 Ljubljana, Slovenia
e-mail: info@fkkt.uni-lj.si

⁵ Guangzhou University, School of Civil Engineering
Guangzhou 510006, China

SUMMARY: To promote the understanding of shrinkage related behaviour of concrete used for tunnel linings the experimental and theoretical investigation including numerical and analytical approach was performed on ring-shaped specimens. Overall one analytical (an.) and two numerical models, namely (i) and (ii) were also developed. Models (an.) and (i) considered the restraining steel ring to be rigid, thus not exhibiting any deformation. Numerical model (ii) considered the steel ring to be deformable. The experimental set-up consisted of a large concrete ring with an inner diameter of 120 cm, an outer diameter of 160 cm and 20 cm in height. The restraining steel ring was 5.5 cm thick. Two concrete rings were made, namely R1 with a low compressive strength of ~26 MPa and the other, R2, with medium compressive strength of ~40 MPa. The strain was measured in the hoop direction on the inner circumference of the steel ring and on the outer circumference of the concrete ring. Concrete rings were subjected to circumferential drying. Numerical model (ii) predicted critical time to the formation of the first crack to be between 13 and 14 days. The experimentally determined critical time is found to be 11 to 13 days with cracks gradually opening over several days. This was indicated by changes in measured concrete and steel strain. Modelled concrete strain just before cracking was between -20 and $-30 \times 10^{-6} \text{ m m}^{-1}$ however, measured concrete strain was $\sim 150 \times 10^{-6} \text{ m m}^{-1}$. Modelled steel strain was between -30 and $-40 \times 10^{-6} \text{ m m}^{-1}$ while measured steel strain was between -10 and $20 \times 10^{-6} \text{ m m}^{-1}$. These discrepancies, in particular the positive steel strain obtained in experiments, require further investigation and improvements of the experimental set-up.

KEY WORDS: Concrete; tunnel lining; restrained shrinkage; Reissner beam theory; modelling.

1 INTRODUCTION

The concrete lining is applied in tunnels to resist the ground and water pressure. The lining is either cast-in-situ or constructed from the precast segments. It is important to apply the lining immediately after the excavation of a tunnel section to protect workers and equipment from the cave-ins or collapse of the unstable ground. The first protective lining is often applied by spraying concrete directly onto the walls of the excavated cavity where concrete sets and hardens, thus creating a protective layer. During the hardening process concrete shrinks due to chemical reactions and water evaporation. Shrinkage is restrained by the underlying rock or soil leading to stress gradients and cracking of the concrete layer. To further the understanding of the restrained shrinkage an analytical model based on the Reissner's beam theory has been proposed and presented by Hozjan et al [1]. The next milestone in this study is data collection via an experimental set-up and model verification.

The common method for measuring concrete shrinkage utilises a non-restrained beam. This method is implemented in standards like Australian standard AS 1012.13 [2] and European norm EN 12390-16 [3]. However, as stated by the *Concrete Institute of Australia*, relations between unrestrained and restrained shrinkage are complex with restrained shrinkage being less than unrestrained [4, p.25]. Therefore, various experimental configurations, summarized by Carlswärd [5], have been proposed to simulate concrete cracking under restrained shrinkage conditions, each with their own set of limitations and drawbacks. However, as can be seen from the work conducted by Weiss and his associates [6]–[8] the restrained shrinkage ring is being recognized as a good value-for-money test, owing to its simplicity, versatility and quantity of derived information.

Standard test implementing this method is American standard ASTM C 1581 [9] which is suitable for mortar and concrete with a maximum aggregate size of 13 mm. The ring specimen used in this test is rather small with the inner diameter, height and wall thickness being 33, 15 and 3.8 cm respectively. These dimensions are too small for sprayed concrete and therefore, a large shrinkage ring set-up is adopted in this study, with the inner diameter of the concrete ring being 120 cm and the outer diameter being 160 cm, yielding wall thickness of 20 cm [10]. The restraining element in this set-up is a steel ring located inside the concrete specimen. Strain measurements were taken on the inside of the steel ring and on the perimeter of the concrete ring, both in the hoop direction.

The main aim of this paper is to present the experimental results of the restrained shrinkage test carried out on two concrete rings, one with low and the other with medium strength concrete. Additionally, the analytical model reported in [1] is summarized and compared to a recently developed numerical model. Experimental results are assessed in terms of their suitability for model verification and the need for further improvements is discussed. Development of the presented shrinkage models aims to enhance the understanding of problems related to the cracking of concrete lining in tunnels.

2 EXPERIMENTAL

The large restrained shrinkage ring consists of a pedestal with push-up hydraulic supports. Plywood sections are placed onto the pedestal so that together with the supports in a retracted position they constitute the base part of the formwork. Steel ring with an outer diameter of 120 cm, the height of 20 cm and the wall thickness of 5.5 cm is placed onto the pedestal. A metal strip, folded into a circle with a diameter of 160 cm, is laid concentrically around the steel ring with spacers keeping the metal strip 20 cm from the steel ring at any point. Metal strip and steel ring thus constitute the vertical part of the formwork into which the concrete is cast. Once concrete sets and gains enough strength to support its own weight it is possible to use the push-up supports to lift the concrete and steel ring from the base and expose the bottom surface to drying. In this experiment, the concrete ring was exposed to circumferential drying only. Main parts of the restrained shrinkage test set-up are shown in a labelled photograph in Fig. 1a.

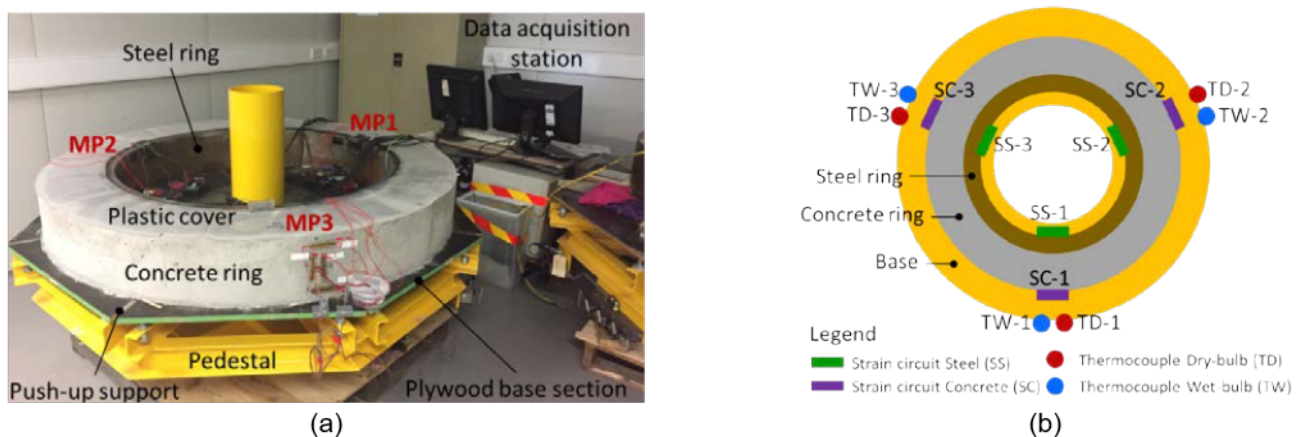


Figure 1: Experimental setup showing (a) photograph of the station with its parts labelled, and (b) schematics of measurement positions and instrumentation arrangement. “MP” stands for Measurement Position.

There are three measurement positions (MP) located circumferentially with 120° angle between adjacent points. Each MP consists of (1) a pair of thermocouples, (2) steel strain-gauge circuit, and (3) concrete strain-gauge circuit. Instrumentation arrangement is schematically presented in Fig. 1b. Thermocouples are attached to the base with a tip

situated half-height of the concrete ring. One serves as a dry-bulb and the other as a wet-bulb temperature gauge allowing for temperature and relative humidity measurements. Both, steel and concrete strain-gauge circuits are wired in a Wheatstone half-bridge configuration. The active arm of the circuit consists of two strain-gauges wired in a series and attached in the hoop direction. Two dummy strain-gauges are wired in a series onto the adjacent arm of the Wheatstone bridge. Such a configuration allows for temperature compensation. In the case of concrete, dummy strain gauges were attached vertically onto the concrete ring while in the case of steel they were attached on a separate steel plate which was placed in thermal contact with the steel ring. Wheatstone bridge was completed with resistors so that resistance of each arm was 240 Ω. All instruments were connected to a data logger *dataTaker DT800* programmed with *DeLogger* [11] software. Data were recorded every 30 s where each recorded value was an average of 30 measurements taken at 1 s intervals.

The experiment was set up in an air-conditioned room with a constant temperature of 20 ± 2 °C and relative humidity ranging between 60 and 80 %. Concrete was manually placed into the formwork and compacted by the means of poker vibrators. Spacers, holding the metal strip in place, were gradually removed and the gaps were filled with concrete. The surface was trowelled and covered with plastic to prevent evaporation. In addition, accompanying cylindrical specimens with a nominal diameter of 10 cm and a nominal height of 20 cm were cast as per AS 1012.8.1 [12]. These specimens were demoulded ~24 h after casting, wrapped in plastic and stored next to the shrinkage ring. They were used for determination of compressive strength and modulus of elasticity preferably on the day the first crack was observed.

The external circumference of the steel ring was lined with plastic to prevent adhesion of concrete to steel and therefore friction-related strain was assumed negligible. The metal sheet, which was removed ~24 h after casting, was coated with formwork lubricant. The concrete ring thus produced had an inner diameter of 120 cm while its thickness and height were 20 cm. In this experiment, the concrete ring was not lifted. Formwork base prevented drying through the bottom and plastic sheet prevented drying through the top. Hence, the concrete ring was exposed to circumferential drying only. Concrete strain-gauges were attached after demoulding. First, a hand-held grinder was used to remove the mortar layer locally at the three MP locations. Next, compressed air was used to blow off the dust particles and dry the surface. Finally, the surface was cleaned with ethanol and strain-gauges applied using CN-E adhesive from *Tokyo Measuring Instruments Lab*.

Two concrete rings, namely R1 and R2, each with its own mix design, were tested. Concrete mix design and properties of the constituent materials are given in Table 1. Concrete was prepared in a laboratory concrete pan mixer in two 110 L batches for each specimen. Cement was General Purpose (GP) type as defined by AS 3972 [13] and fly ash was Grade 1 according to AS 3582.1 [14]. Manufactured sand and coarse aggregate particles had angular grains while the grains of the river and fine sand were round. The aggregate composition was optimised using the particle size distribution data. All aggregates were dried before use.

Table 1: Properties of concrete components mix design for concrete rings R1 and R2 used in the restrained shrinkage test. Mix design is given as mass of components required for 1 m³ of concrete.

Concrete components and their properties					Concrete mix design (kg per 1 m ³ of concrete)	
Material		Symbol	Density (kg m ⁻³)	Water absorption (wt%)	R1	R2
Powders	Cement	C	3.12	---	214	315
	Fly Ash	FA	2.35	---	92	105
Aggregates	Crushed 10 mm	CA10	2.89	0.28	775	751
	Manufactured Sand	MS	2.91	0.56	388	376
	River Sand	RS	2.66	1.78	485	470
	Fine Sand	FS	2.65	0.67	291	282
Water		W	1.00	---	199	174
Superplasticizer		SP	1.07	---	---	4.2

The idea underlying the concrete mix selection was to design two workable mixes with approximately the same volumetric fraction of paste, one mix with high water content and low strength (R1) and the other with lower water content and higher strength (R2). Namely, in a concrete system, it is the hardened paste that undergoes drying shrinkage while the aggregate is considered dimensionally stable. As can be seen in Table 2, R2 contained 2 vol% more paste than R1

however, R1 paste contained more water per unit of powder material with effective water-powder ratio (WP-eff) being 0.60 for R1 and 0.38 for R2.

Table 2: Concrete mix parameters. Dosage of powders (DP) gives a total mass of active powders per 1 m³ of concrete. Absolute water-powder ratio (WP-abs) accounts for all water added to the mix while effective water-powder ratio (WP-eff) disregards water absorbed by the aggregates. Designed compressive strength is the strength expected at 28 days on specimens subjected to standard curing.

Attributes	Symbol	Unit	R1	R2
Dosage of powders	DP	kg	306	420
Water-powder ratio Absolute	WP-abs	kg kg ⁻¹	0.65	0.41
Water-powder ratio Effective	WP-eff	kg kg ⁻¹	0.60	0.38
Paste content	f_p	vol%	31	33
Designed 28-day compressive strength	σ_N	MPa	30	60

3 MODELLING

To understand the measured properties and their relation to geometric and material characteristics of the experimental set-up, two mathematical models – one analytical and the other numerical, were developed.

3.1 Analytical model

The analytical method based on the Reissner's geometrically exact beam theory [15] is applied to solve the steel-concrete ring problem. The analytical method, including a system of ten governing equations, namely the equilibrium, kinematic and constitutive equations, and the corresponding boundary conditions, is derived and explained in detail in [1] and [16]. The analytical method assumes a rigid and non-deformable steel ring, no shear strain in the concrete ring and no separation of the concrete and steel rings, enabling only an interlayer slip. The total strain in the concrete ring in the tangential direction ε_c is determined as a sum of the mechanical strain ε_m and the strain due to the shrinkage of concrete ε_{cs} as

$$\varepsilon_c = \varepsilon_m + \varepsilon_{cs} \quad (1).$$

Time development of the strain due to shrinkage of concrete is applied in accordance with Eurocode 2 (EN 1992-1-1 [17]). Since the concrete ring does not deform until the first crack is formed, the analytical method yields the following equation

$$\sigma = E \varepsilon_m = -E \varepsilon_{cs} \quad (2),$$

where σ denotes the tangential stress in the concrete ring and E the elastic modulus of concrete. Since the strain due to the shrinkage of concrete, ε_{cs} in Eq. (2), is a negative quantity, the stress in the concrete ring, σ , is tensile and the first crack forms when the tensile stress in the concrete ring is larger than the tensile strength of concrete f_{ct}

$$\sigma_{cr} = -E \varepsilon_{cs,cr} \geq f_{ct} \quad (3),$$

where σ_{cr} and $\varepsilon_{cs,cr}$ denote the critical stress and the critical strain due to the shrinkage of concrete, respectively. The corresponding critical time is denoted t_{cr} . The location of the first crack is arbitrary since a geometrically and materially perfect concrete ring is considered. Stiffness of the contact between the concrete and the steel ring does not influence the stress in the concrete ring until the formation of the first crack. At any given time, the stress and strain fields are uniform across the concrete and the steel ring, however, they change over time.

3.2 Numerical model

The problem of the restrained shrinkage of the concrete ring is numerically solved using the finite element software COMSOL *Multiphysics* [18]. Two models were devised to separately solve (i) the problem of the restrained shrinkage of concrete by a rigid and non-deformable steel ring, and (ii) the problem of restrained shrinkage of concrete by a deformable steel ring. Model (i) is directly comparable to the analytical model. The influence of the deformable steel ring on the shrinkage of the concrete ring is studied in model (ii). Both problems are modelled in two dimensions (2D) since

the lateral deformations are small compared to the total axial (tangential) deformations of the concrete ring, ε_c . Symmetry is applied and therefore only half of the concrete and the steel ring is modelled. Both materials are considered isotropic and linearly elastic. Measured material parameters were used for modelling. These were determined experimentally as explained in ch. 2 and results are stated in ch. 4. The solution is obtained by the constant Newton method. A generalized alpha method is used for time discretization. A 2D numerical domain was meshed to 1450 triangular second-order (quadratic) isoparametric Lagrangian elements. The stress in the concrete ring, σ , as well as the strain in concrete, ε_c , and steel rings, ε_s , are calculated at time steps of 0.1 day.

3.3 Analytical and numerical model forecast

Stress development in the concrete ring, σ , over time, t , determined by the analytical method (an.) and numerical models (i) and (ii) is presented in Fig. 2. Figure 2a compares the analytical model (an.) and the numerical results of model (i) for concrete mixes R1 and R2. It can be seen that the numerical results agree well with the results of a relatively simple, but accurate, analytical model. Figure 2b shows the numerical results of stress development over time for model (ii) where shrinkage of the concrete ring is restrained by the deformable steel ring. The horizontal solid lines in Figs. 2a and 2b denote the estimated tensile strength of concrete, namely $f_{ct} = 1.8$ MPa for R1 (blue lines) and $f_{ct} = 2.3$ MPa for R2 (red lines). Tensile strength was estimated based on measured compressive strength using the equation given in AS 3600 [19]. The corresponding critical time, t_{cr} , at which the first crack forms, is marked with vertical dashed black lines. Analytical method (an.) and model (i) show the critical time to be 9 and 8 days for R1 and R2, respectively while model (ii) yields 14 days for R1 and 13 days for R2 which is 5 days more than models (an.) and (i).

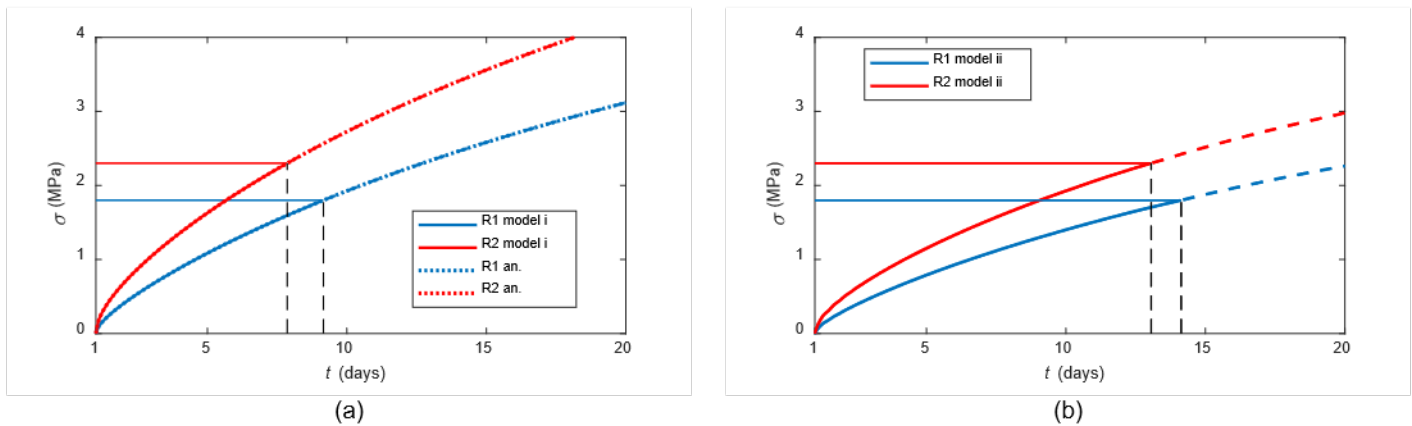


Figure 2: Time development of the stress in the concrete ring, σ , determined by (a) numerical model (i) and the analytical method (an.), and (b) the numerical model (ii) for R1 and R2 concrete. The horizontal solid lines denote the tensile strength of concrete, $f_{ct} = 1.8$ MPa for R1 (blue line) and $f_{ct} = 2.3$ MPa for R2 (red line). Vertical black dashed lines denote the corresponding critical time, t_{cr} .

Strain development in the concrete ring, ε_c , and steel ring, ε_s , over time, t , determined by the model (ii) is presented in Fig. 3. Vertical dashed black lines denote critical time as found by model (ii) in Fig. 2b. The corresponding strain is marked by the horizontal solid lines, namely blue line for R1 and red line for R2. The strain in the concrete ring, ε_c , just before the formation of the first crack, is found in Fig. 3a with values of $-22 \times 10^{-6} \text{ m m}^{-1}$ for R1 and $-27 \cdot 10^{-6} \times 10^{-6} \text{ m m}^{-1}$ for R2. The resulting strain in the steel ring, ε_s , is shown in Fig. 3b and its values are roughly in the same range, namely $-30 \times 10^{-6} \text{ m m}^{-1}$ for R1 and $\varepsilon_s = -38 \times 10^{-6} \text{ m m}^{-1}$ for R2.

Note that the stress and strain in Figs. 2 and 3 are plotted as dashed lines for $t > t_{cr}$ to potentially enable a determination of t_{cr} for different values of f_{ct} , however, the stress instantly reduces to zero and the strain relaxes to a smaller value at the formation of the first crack. The analytical method and the numerical modelling also give equal lengths of the first crack that are 0.11 and 0.12 mm for the concrete mixes R1 and R2, respectively, when a smooth sliding between the concrete and the steel rings is considered.

4 RESULTS AND DISCUSSION

Time of the first sighting of the crack and concrete properties measured on cylinders are summarized in Table 3. Measured compressive strength and modulus of elasticity were used in analytical and numerical modelling. Crack on R1

was observed rather late which was due to concrete having low strength and thus soft failure which resulted in a small width of the crack. Therefore, time to the first sighting of the crack in R1 is most likely longer than the actual appearance of the crack. For R2, daily visual inspection was carried out with a magnifying glass and a torch therefore time to the first sighting of the crack more accurately presents the time of the cracking.

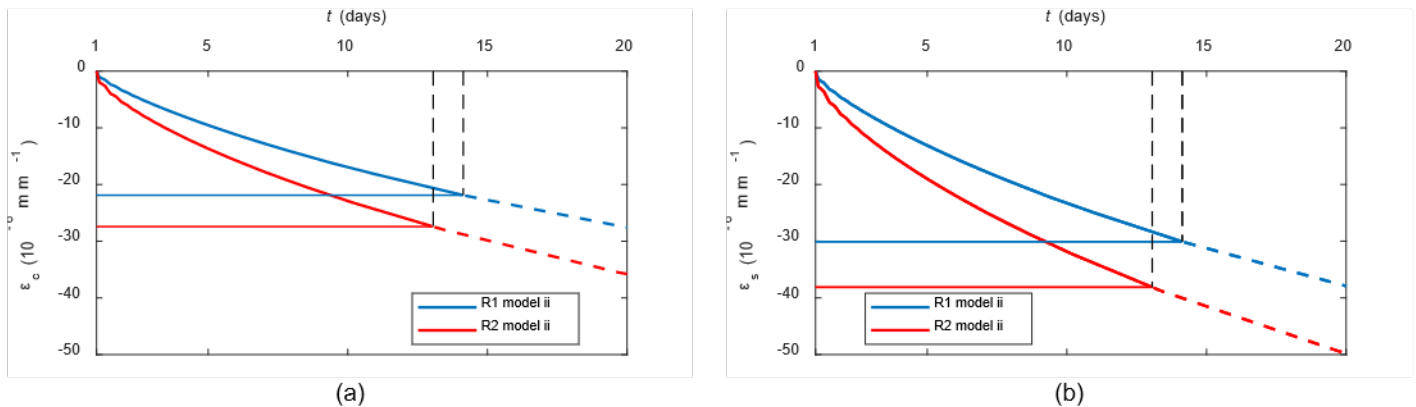


Figure 3: Time development of the strain in a) concrete ring, ϵ_c , and b) steel ring ϵ_s , determined by the numerical model (ii) for R1 and R2 concrete. The vertical black dashed lines denote the critical time, t_{cr} . The corresponding strain in the concrete, ϵ_c , and the steel, ϵ_s , rings are marked with the horizontal solid lines for the mixes R1 (blue line) and R2 (red line).

Table 3: Properties of concrete R1 and R2 at the time when the crack on restrained shrinkage ring was observed. The average value and sample standard deviation are stated. Sighting of the crack refers to the time the crack was visually spotted on the concrete ring and does not necessarily correspond to the first formation of the crack.

Concrete property	Symbol	Unit	R1	R2
Time to the first sighting of the crack	t	days	14	11
Time of tests on cylinders	t_c	days	20	11
Density	ρ_c	kg m^{-3}	2370 ± 20	2440 ± 10
Compressive strength	σ_c	MPa	26 ± 2	40 ± 5
Modulus of elasticity	E_c	GPa	31 ± 4	35 ± 5

Strain measured on steel ring for R1 and R2 is shown in Fig. 4 (a-b). Strain measurements on concrete were not successful for R1 due to problems with strain-gauge adhesion and data acquisition system. These problems were resolved for R2 by using compressed air not only to clean but also to locally dry the surface and by reprogramming the data acquisition system. Therefore, strain development in R2 concrete is shown in Fig. 4 (c).

Steel strain vs time diagrams in Fig. 4 (a-b) show a drop of strain, which indicates the formation of cracks, between 11 and 12 days after casting for R1 and between 13 and 17 days for R2. This is in agreement with the observations in Fig. 4 (c) showing a drop of concrete strain for R2 between 14 and 17 days. While the critical time, t_{cr} , predicted by the numerical model (ii) is within the same range as the actual measurements, the model predicted a shorter critical time for R2 than for R1. In this respect it should be noted, that development of macro crack on such a large ring is gradual and it happens over several days which is not accounted for by modelling.

The concrete strain measured on R2 at the time the cracking started, was negative, indicating contraction, with values being between $\sim(-180 \text{ to } -130) \times 10^{-6} \text{ m m}^{-1}$. These values are ~ 5 -times the values predicted with the numerical model (ii). The steel strain, on the other hand, was measured to be between $\sim(10 \text{ to } 20) \times 10^{-6} \text{ m m}^{-1}$ which in absolute terms is approximately half of the predicted value. However, steel strain is positive, indicating extension, which is an unexpected outcome of the test. In this respect, it is important to note that in both experiments steel strain SS-1 is negative for the first two days dropping to a value of $\sim(-7 \times 10^{-6} \text{ m m}^{-1})$ before starting to increase. Furthermore, three discontinuities are observed in SS-1 curve on R2 (Fig. 4b) which may indicate slippage.

Temperature and relative humidity measurements obtained by dry and wet-bulb thermocouple are summarized in Fig. 5. Peaks observed in temperature measurements in R1 experiment (Fig. 5a) are due to the influx of air when the door opened, however, the temperature stabilized promptly and was fairly constant between 19 and 21 °C. This is within the room parameters of 20 ± 2 °C. A protective screen placed in front of the door resolved this issue in experiment R2, thus

temperature peaks in Fig. 5b are smaller. Humidity measurements encountered additional problems in R1 experiment since the wet-bulb thermocouple dried out frequently. This is observed in Fig. 5c as relative humidity curve plateauing at 100 %. This problem was resolved in R2 experiment and therefore such anomalies are not found in Fig. 5d. Nevertheless, the relative humidity was found to fluctuate between 40 and 80 % which is somewhat outside the room set parameters of 60 to 80 %. When comparing graphs in Figs. 4 and 5 no direct link between temperature and relative humidity fluctuations and strain measurements is found. Still, narrowing down the range of relative humidity fluctuations needs to be considered in future experiments.

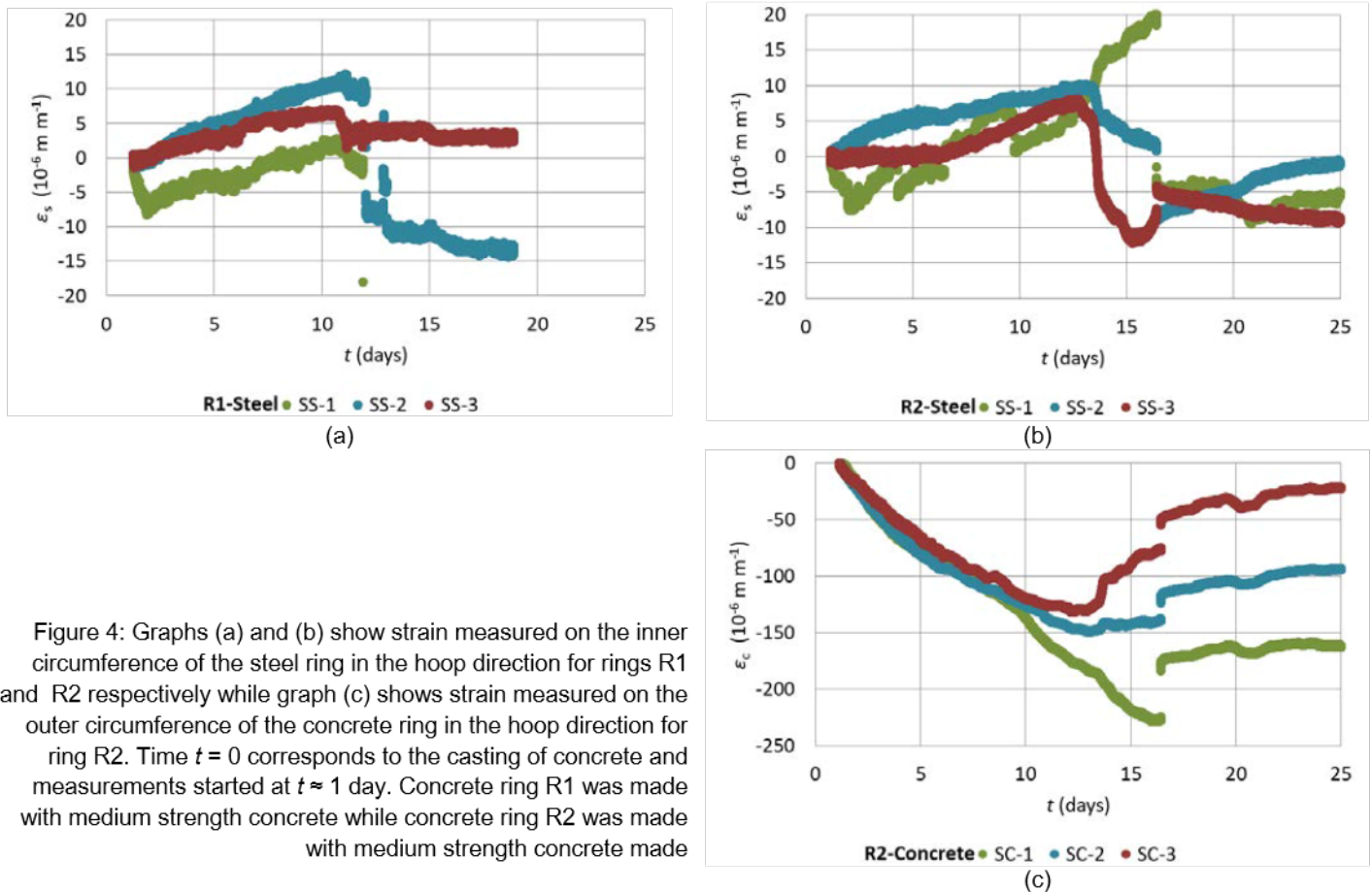


Figure 4: Graphs (a) and (b) show strain measured on the inner circumference of the steel ring in the hoop direction for rings R1 and R2 respectively while graph (c) shows strain measured on the outer circumference of the concrete ring in the hoop direction for ring R2. Time $t = 0$ corresponds to the casting of concrete and measurements started at $t \approx 1$ day. Concrete ring R1 was made with medium strength concrete while concrete ring R2 was made with medium strength concrete made

While the experimental results are promising they clearly show the need for further refinements of the test set-up. The configuration of the strain-gauges could be improved by installing independent strain-gauge circuits at the bottom, middle and at the top of the ring. This would enable capturing the variability in the vertical stain profiles due to pressure gradients which arise from drying as shown by Moon [8]. Steel strain gauge measurements should be validated by applying equal pressure on the whole circumference and by checking the quality of Wheatstone bridge thermal compensation. Furthermore, the interface between steel and concrete should be investigated for any friction and additional measures should be taken to reduce it. Sealing of the top surface could be improved by using paraffin vax or silicon cover instead of plastic. While the relative humidity measured in the vicinity of the concrete ring fluctuated between 40 and 80 %, no direct correlation was observed with fluctuations in strain measurements. Nevertheless, the experimental set-up should be moved to a humidity-controlled room.

5 CONCLUSIONS

An experiment was conducted in conjunction with the proposed analytical and numerical models aiming to enhance the understanding of restrained shrinkage of concrete. Based on the ring geometry, properties of concrete and steel and by using the equation provided by Moon [8, p.48, Eq.3.6], the degree of restraint was estimated to be ~ 70 %. Two concrete rings, R1 and R2, were made. Their compressive strength was ~ 26 MPa and ~ 40 MPa respectively at the time of the crack sighting. Concrete rings were subjected to circumferential drying. The resulting strain was measured in the hoop direction on the inner circumference of the steel ring and on the outer circumference of the concrete ring. While

experimental data is promising, several issues need to be resolved. Most important is the positive strain measured on the steel ring. It is recommended to instal three independent Wheatstone bridges at each MP, namely one at the bottom, one at the middle and one at the top of the steel ring. Measurements on these strain gauges should be validated by applying controlled uniform pressure on the whole circumference of the steel, for example by using a pneumatic airbag system. Unrestrained shrinkage should be measured on companion specimens to provide additional data for modelling. It might be beneficial to use mature concrete blocks, whose moisture content is in equilibrium with the test room, for dummy strain-gauges in concrete Wheatstone bridges. Further measures should be taken to prevent any slippage between steel and concrete ring and to prevent top and bottom drying.

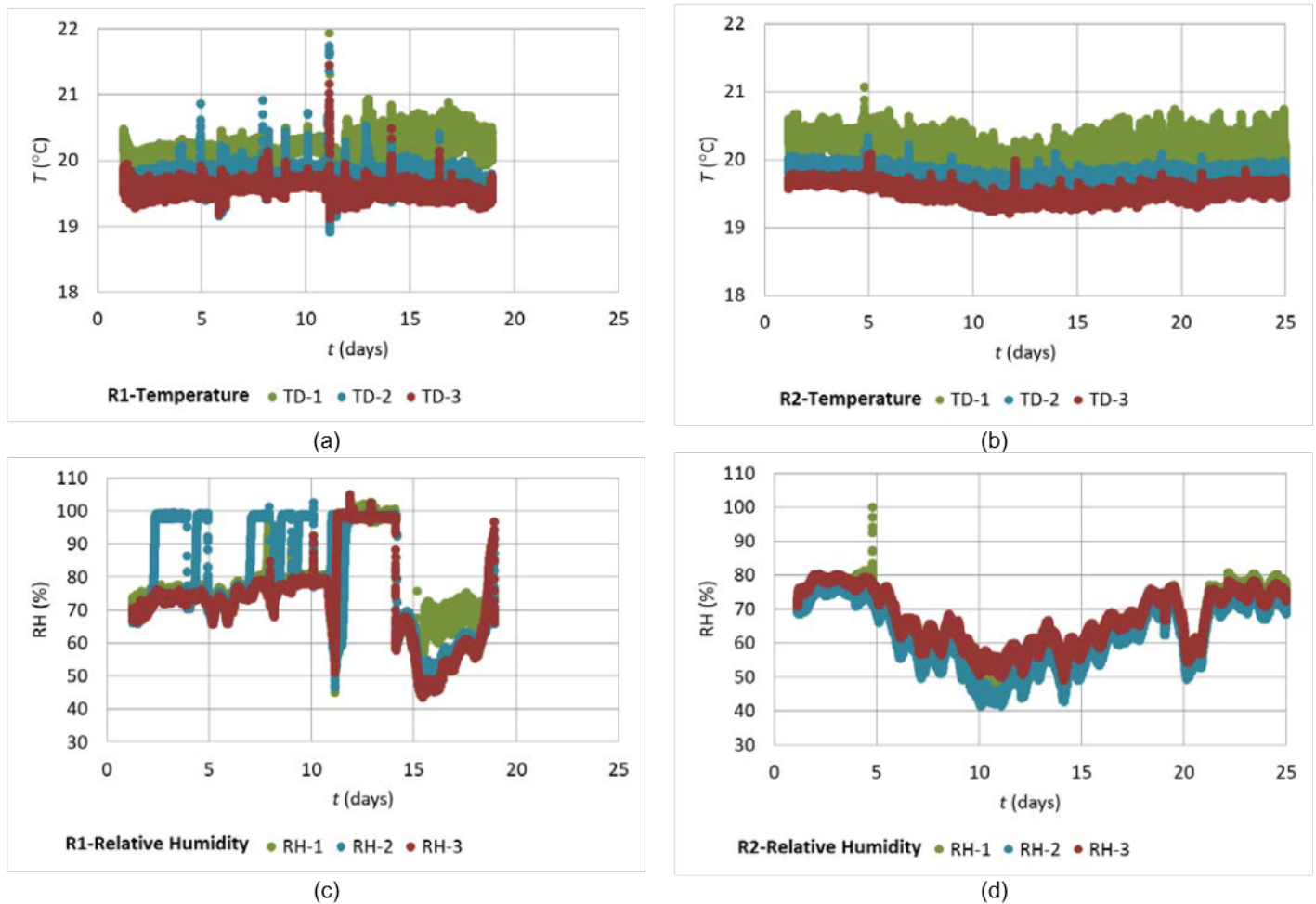


Figure 5: Graphs (a) and (b) present temperature measurements and graphs (c) and (d) present relative humidity measurements carried out at the three measuring points for rings R1 and R2 respectively. Ring R1 was made with low strength concrete while ring R2 made with medium strength concrete. Time $t = 0$ corresponds to the casting of concrete while measurements started at $t \approx 1$ day.

ACKNOWLEDGEMENTS

The authors would like to acknowledge the contribution of Mr Adrian Chau for initial equipment performance tests conducted in the scope of his bachelor's thesis at *The University of Queensland* (UQ). Technical support of Mr Jason Van Der Gevel, Mr Stewart Matthews and Mr Shane Walker (all School of Civil Engineering, UQ), as well as consultancy provided by Mr Peter Bleakley (instrumentation Workshop, UQ), are greatly appreciated. T. Hozjan and I. Planinc acknowledge the supported by the *Slovenian Research Agency* through the research core funding No. P2-0260.

REFERENCES

- [1] Hozjan T.; Karlovšek, J.; Hanžič, L.; Huč, S.; Planinc, I.: Analytical method for determination of crack development in concrete ring due to restrained shrinkage, in *Advancements in Civil Engineering and Architecture*, 2019, vol. 1: Civil Engineering, pp. 1381–1389.

- [2] AS 1012.13 Methods of testing concrete. Determination of the drying shrinkage of concrete for samples prepared in the field or in the laboratory. *Standards Australia*, 2015.
- [3] EN 12390-16 Testing hardened concrete. Determination of the shrinkage of concrete. *European Committee for Standardization (CEN)*, 2019.
- [4] Shotcreting in Australia: recommended practice. *Concrete Institute of Australia*, 2010.
- [5] Carlswärd, J.: Shrinkage cracking of steel fibre reinforced self compacting concrete overlays - Test methods and theoretical modelling, PhD thesis. *Luleå University of Technology*, Luleå, Sweden, 2006.
- [6] Weiss, W. J.; Yang, W.; Shah, S. P.: Influence of specimen size/geometry on shrinkage cracking of rings, *Journal of Engineering Mechanics*, 126 (2000)1, pp. 93–101.
- [7] Hossain, A. B.; Weiss, J.: Assessing residual stress development and stress relaxation in restrained concrete ring specimens, *Cement and Concrete Composites*, 26 (2004) 5, pp. 531–540.
- [8] Moon J. H.: Shrinkage, Residual Stress and Cracking in Heterogenous Materials, PhD thesis. *Purdue University*, West Lafayette, Indiana, 2006.
- [9] ASTM C1581 Standard test method for determining age at cracking and induced tensile stress characteristics of mortar and concrete under restrained shrinkage. *ASTM*, 2009.
- [10] Raoufi, K.; Bernard, E. S.; Weiss, W. J.: Shrinkage cracking behavior of fiber reinforced concrete: as assessed using the restrained ring test, *Journal of ASTM International*, 7 (2010) 7, pp. 1–15.
- [11] *DeLogger* 5.0, dataTaker, Industrial Temperature Sensors Ltd, 2012.
- [12] AS 1012.8.1 Methods of testing concrete. Method for making and curing concrete. Compression and indirect tensile test specimens. *Standards Australia*, 2014.
- [13] AS 3972 General purpose and blended cements. *Standards Australia*, 2010.
- [14] AS 3582.1 Supplementary cementitious materials. Fly ash. *Standards Australia*, 2016.
- [15] Reissner, E.: On one-dimensional finite-strain beam theory: The plane problem, *Journal of Applied Mathematics and Physics*, 23 (1972), pp. 795–804.
- [16] Hozjan, T.; Saje, M.; Srpčič, S.; Planinc, I.: Geometrically and materially non-linear analysis of planar composite structures with an interlayer slip, *Computers and Structures*, 114 (2013), pp. 1–17.
- [17] EN 1992-1-1 Eurocode 2: Design of concrete structures General rules and rules for buildings. *European Committee for Standardization (CEN)*, 2014.
- [18] *COMSOL Multiphysics* 5.5, COMSOL, 2019.
- [19] AS 3600 Concrete structures. *Standards Australia*, 2018.